

Research Article

Optical Design and Simulation of Snapshot Hyperspectral Dental Imaging Spectrometer with One-Dimensional Random Coding

Jiajing Cao ¹, Jun Chang ¹, Yi Huang¹, Wenxi Wang¹, Xinran Guo¹ and Shangnan Zhao²

¹Key Laboratory of Photoelectronic Imaging Technology and System of Ministry of Education of China, School of Optics and Photonics, Beijing Institute of Technology, Beijing 100081, China

²Key Laboratory of Optical System Advanced Manufacturing Technology, Changchun Institute of Optics, Fine Mechanics and Physics, Changchun 130033, China

Correspondence should be addressed to Jun Chang; optics_chang@126.com

Received 21 December 2022; Revised 3 February 2023; Accepted 12 April 2023; Published 20 April 2023

Academic Editor: Thomas Walther

Copyright © 2023 Jiajing Cao et al. This is an open access article distributed under the Creative Commons Attribution License, which permits unrestricted use, distribution, and reproduction in any medium, provided the original work is properly cited.

To achieve perfect teeth color reproduction, we propose the design of a snapshot hyperspectral imaging spectrometer that can accurately measure the teeth spectrum. In this paper, the optical system of a snapshot hyperspectral dental imaging spectrometer is designed. In particular, to encode images in both the spatial and spectral dimensions, a one-dimensional random coding mask rotated 45 degrees around the optical axis is used. The system has a spectral resolution of approximately 2.2~10 nm in the 450~700 nm spectral range, and the total length of the system is less than 150 mm. The whole design can be used as a miniaturized handheld instrument. To verify the feasibility of whiteness measuring, a simulation experiment is carried out. The target spectral information is reconstructed through the reconstruction algorithm. The simulation result shows that spectral imaging has the potential to improve the accuracy and precision of teeth whiteness measurements.

1. Introduction

Teeth repair and whitening have received much attention in recent years due to their aesthetics. To measure the whiteness of teeth or dentures accurately, many efforts have been made to accurately measure the whiteness of teeth. Traditionally, shadow guidelines [1] can be used for visual evaluation of teeth whiteness when arranged from light to deep. However, the visual evaluation of teeth also has certain limitations, such as the influence of light or the surrounding environment [2]. Therefore, digital technology with low subjectivity and high accuracy is increasingly favored.

Under regular circumstances, chromaticity matching in digital photography [3] is a workable measurement technique. The use of an intraoral camera [4] with LED and cross-polarized lighting [5] can eliminate the effects of ambient lighting [6] and unfixed object-camera distance. Additionally, new shade matching techniques have been used to increase color measurement accuracy [7]. A colorimeter [8] simulates an object's color using the responses

of three glass filters (red, green, and blue). Dental spectrophotometry [9], which holds a dominant position in teeth color assessment methods, complements the aforementioned two techniques by measuring color through assessing the spectral reflectance or transmittance of objects. For example, SpectroShade Micro spectrophotometer [10, 11] and Olympus's Crystal Eye spectrophotometer [12] combine spectrophotometer with LED lighting source and digital photography technology, allowing for more accurate matching of teeth chroma. However, the measurement results from this instrument are still influenced by tooth position, translucency [13], and probe angle, which requires further study in the future.

The imaging spectrometer, whose principle is similar to that of spectrophotometer, can acquire the image with the entire spectrum information at once, while spectrophotometers need to scan to obtain the intensity of a specific spectral line or a certain segment. In the work of tooth whiteness measurement, the measurement result by using spectrophotometers is more precise and accurate, but the

working speed is slower than that by using imaging spectrometer [14, 15]. Therefore, to improve the measurement speed and improve the user's experience, imaging spectrometer is a better measurement method on the premise of ensuring accuracy.

With the development of imaging spectrometers, there are two types: scanning type and snapshot type. Snapshot imaging spectrometers simultaneously obtain spatial and spectral information on the image plane through regular or irregular transformation of the spatial and spectral information of the target, in contrast to scanning type imaging spectrometers, whose complex structure prevents the miniaturization and lightweight design of the system. There are several ways to compose a snapshot spectrometer. Using a microlens array is one method. For example, Zexia Zhang et al. achieved a snapshot image spectrometer with a 5 nm spectral resolution using a microlens array [16]. By using a geometric phase microlens array, Wang et al. showed a spectrometer with low-cost mass production [17]. Dwight et al. used a tunable microlens array to achieve alterable spectral resolution [18]. Another way is Fourier transform. Based on a snapshot Fourier transform spectrometer, Zhang et al. showed a high-quality panchromatic image acquisition approach [19]. The coding aperture is also a feasible mechanism to reconstruct three-dimensional (3D) spectral data from a single image, which leads to the coded aperture snapshot imaging spectrometer (CASSI) [20]. To reduce the reconstruction difficulty, Wang et al. combined the coded CASSI measurement with the noncoding grayscale measurement [21]. To improve the imaging performance of CASSI system, Zhang et al. proposed an adaptive spatially coded aperture [22]. Among those spectrometers, the structure of CASSI is conducive to the development of low-cost handheld dental spectrometers.

In this paper, a snapshot hyperspectral dental imaging spectrometer is proposed based on the principle of CASSI. Particularly, a one-dimensional random coding mask rotated 45 degrees around the optical axis is used to encode imaging in both spatial and spectral dimensions. The spectral data of teeth can be obtained at one time to achieve the perfect reconstruction of teeth color. The optical system of a snapshot hyperspectral dental imaging spectrometer is designed, and a theoretical simulation experiment is carried out. Finally, the 3D spectral information about simulation target model is reconstructed through the reconstruction algorithm.

2. Principle of the Snapshot Hyperspectral Dental Imaging Spectrometer

Figure 1 shows the optical layout of the snapshot hyperspectral dental imaging spectrometer, which consists of six parts: fore optics, coding mask, collimating lens, dispersion element, focusing lens, and a detector. The image of the target object can be passed through the fore optics to form a primary intermediate image. Then, the primary image is modulated by a one-dimensional coding element. Through the collimating lens, spectral element, and focusing lens, the spectrum modulated image can form a partially overlapping two-dimensional image. To obtain a three-dimensional spectral data cube, the spectral data can be decoded by using the compressed sensing optimization method.

On the basis of the CASSI system mathematical model, a one-dimensional random coding form is adopted, as shown in Figure 2. Particularly, the coding mask is rotated 45 degrees around the optical axis to encode spatial and spectral dimensions, which reduces coding complexity and makes the alignment simpler. The system imaging process can be expressed as follows:

$$\begin{aligned} I_{\text{detector}}(x, y) &= \int I_{\text{object}}(x, y, \lambda) \cdot M_{\text{mask}}(x, y) \cdot p(x, y_{\lambda} \cdot \alpha, \lambda) d\lambda \\ &= \int I_{\text{object}}(x, y, \lambda) \cdot C_{\text{mask}}(x, y_{\lambda}, \lambda) d\lambda, \end{aligned} \quad (1)$$

where $I_{\text{detector}}(x, y)$ represents the target spectral modulation image received by the detector; $I_{\text{object}}(x, y, \lambda)$ represents the target 3D spectral image data; $C_{\text{mask}}(x, y_{\lambda}, \lambda) = M_{\text{mask}}(x, y) \cdot p(x, y_{\lambda} \cdot \alpha, \lambda)$ represents a 3D data cube of the encoded dispersion spectrum; $M_{\text{mask}}(x, y)$ represents the coding modulation function; $p(x, y_{\lambda} \cdot \alpha, \lambda)$ represents the spectral dispersion function; $y_{\lambda} = y + \delta\lambda$ represents the spatial coordinates after dispersion; $\delta\lambda$ represents the difference between the current wavelength and the initial wavelength; and α represents the angular dispersion.

The magnification β of a relay imaging system with a collimating lens and focusing lens affects the value of the coding unit and the spatial resolution. The following formulas can be used to determine the magnification β :

$$\beta = \frac{f_c}{f_s}, \quad (2)$$

where f_c is the focal length of the collimating lens and f_s is the focal length of the focusing lens. Generally, $\beta = 1$.

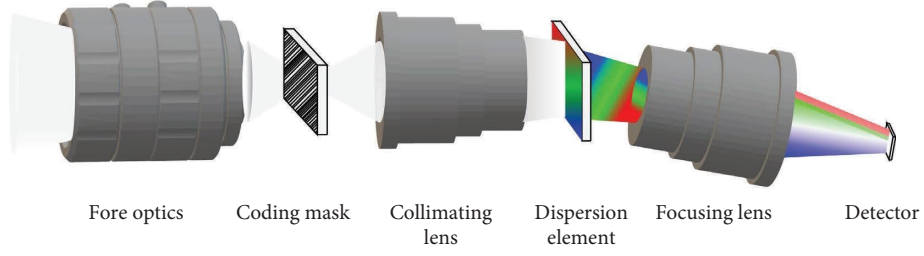


FIGURE 1: Optical layout of the snapshot hyperspectral dental imaging spectrometer.

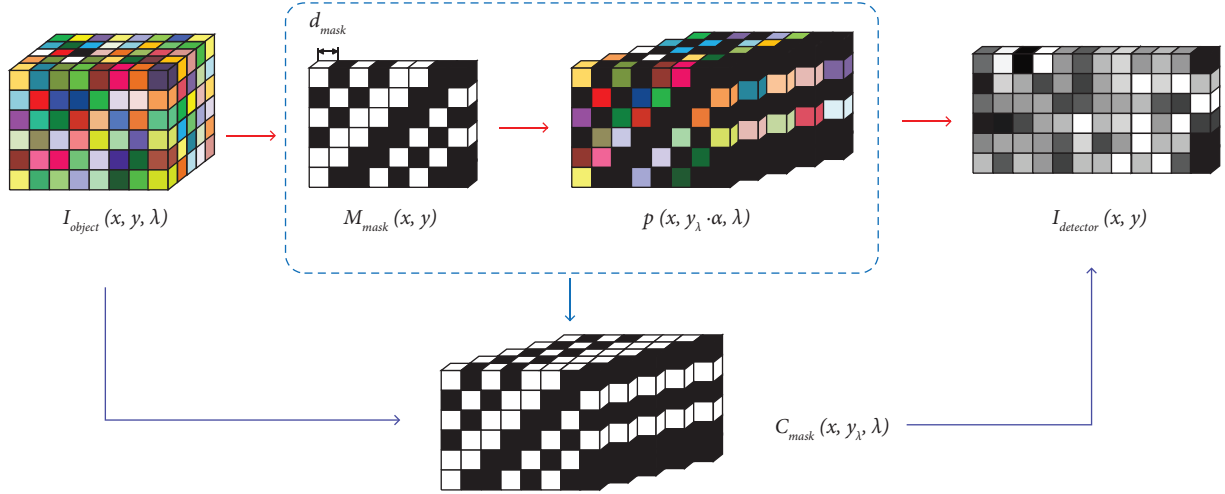


FIGURE 2: The imaging process of the snapshot hyperspectral dental imaging spectrometer.

TABLE 1: Parameters of the snapshot hyperspectral dental imaging spectrometer.

Design parameters		Parameter value
Focal length	Objective	25 mm
	Collimating lens	35 mm
	Focal lens	35 mm
Prism angle		20°
Wavelength range		450~700 nm
Spectral resolution		≤10 nm
Coding unit size		9.6 μm
Coding area		640 * 458

According to the above process, the size of the coding unit affects the spectral resolution of the system, and the relationship between the coding unit and spectral resolution should meet the following requirements

$$d_{\text{mask}} = \beta \cdot \alpha \cdot \Delta\lambda \cdot f_{\text{focus}}, \quad (3)$$

where d_{mask} is the size of the coding unit, f_{focus} is the focal length of the focusing imaging lens group, and $\Delta\lambda$ is the spectral resolution.

In addition, to ensure clear imaging and calibration accuracy of the system, the relationship between the resolution of the coding element and the resolution of the detector should be as follows:

$$\frac{d_{\text{mask}}}{d_{\text{detection}}} = C (C \in \mathbb{Z}, C > 0), \quad (4)$$

where d_{mask} is the size of coding unit and $d_{\text{detection}}$ is the pixel size of the detector. If $d_{\text{mask}} = d_{\text{detection}}$, there is a one-to-one correspondence between the detector pixel and the coding unit. And this is the best relationship for accurate calibration and spectral reconstruction regardless of the value of β .

3. Optical Design of the Snapshot Hyperspectral Dental Imaging Spectrometer

Considering the miniaturization of the system, the surface area of teeth, and the depth of the probe into the mouth, the object-tooth distance range should be 70–120 mm, and the target size should be greater than 15 mm * 15 mm (maximum average crown surface area). To limit the aperture of the beam entering the optical system, the optical system has a real entrance pupil whose diameter is set to 5 mm. To obtain a clear teeth image with a certain height fluctuation,

TABLE 2: The parameters of the two orthogonal toroid surfaces.

Parameters	Surface 1	Surface 2
Radius (mm)	66.354	19.423
Rotating axis	x	y
Rotating radius (mm)	Infinite	Infinite
Conic efficient (k)	0.026164	5.000000
α_2	0.000126	-0.000350
α_3	$-4.70639e-006$	$6.65524e-005$
α_4	$6.80674e-008$	$-4.14135e-006$

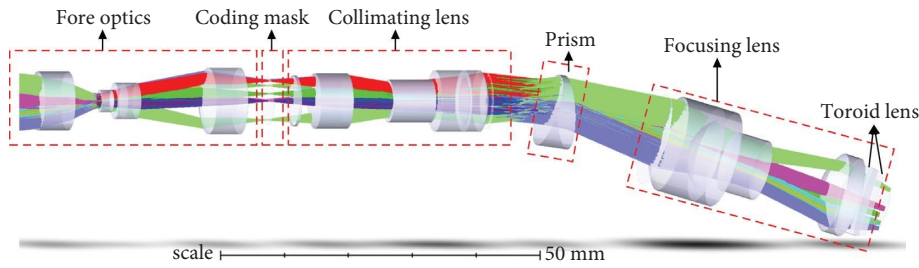
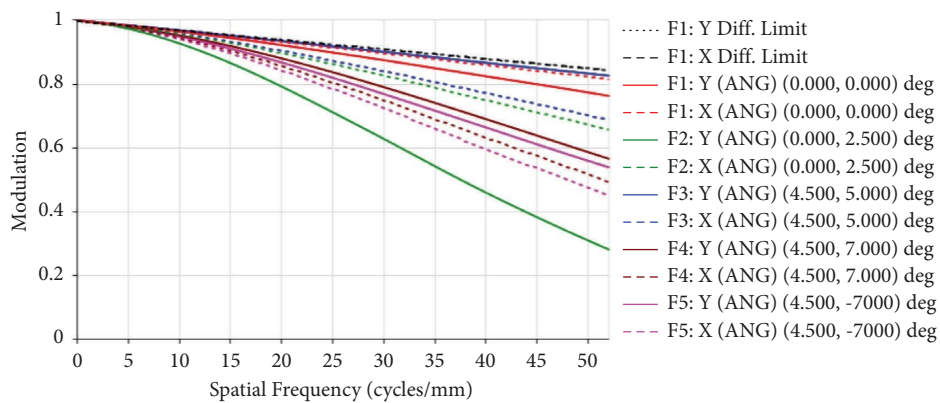
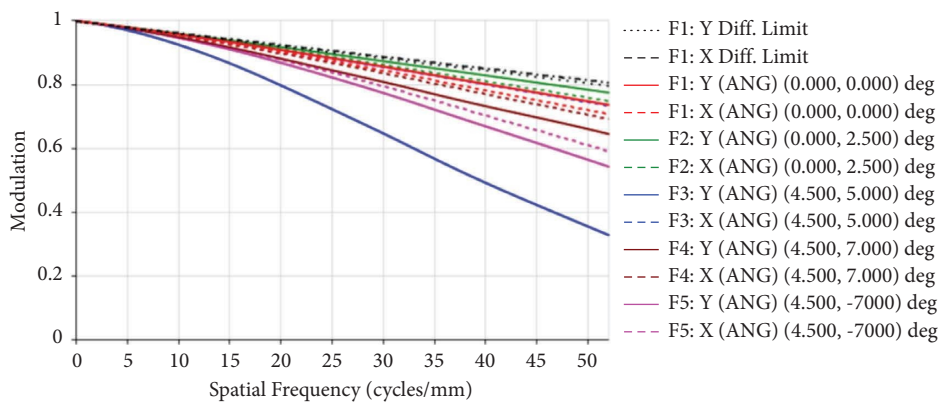


FIGURE 3: Optical layout of the snapshot hyperspectral dental imaging spectrometer.



(a)



(b)

FIGURE 4: Continued.

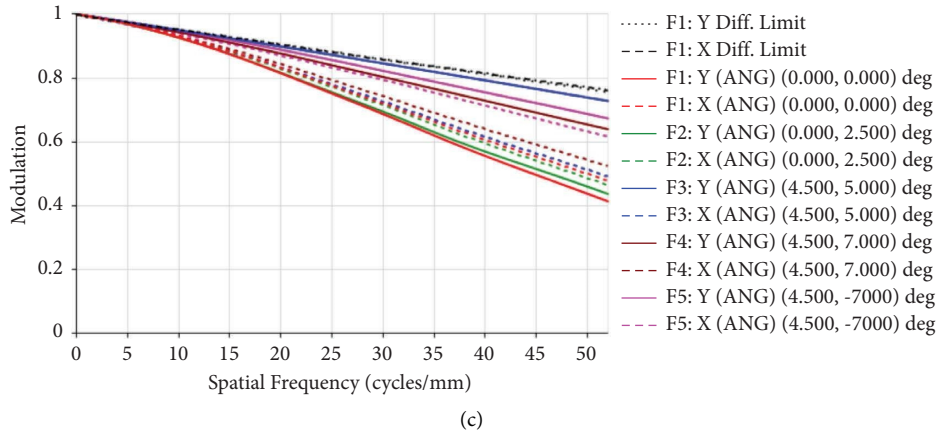


FIGURE 4: MTF of the system at three wavelengths: (a) 450 nm, (b) 570 nm, and (c) 700 nm.

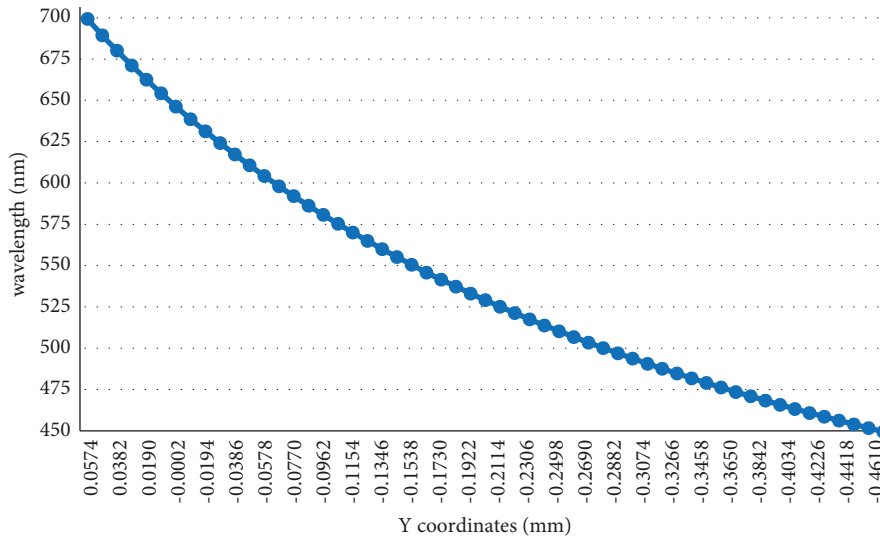


FIGURE 5: The spectral sampling of different dispersion positions.

the system needs to have a large depth of field. That is, the system needs to have a large F number. To accurately characterize teeth whiteness, the spectral range is set to 450~700 nm. Some parameters of the snapshot dental imaging spectrometer are shown in Table 1.

The optical layout of the snapshot hyperspectral dental imaging spectrometer is shown in Figure 3. The field of the system is $14^\circ \times 9^\circ$, the total length of the system is less than 150 mm, and the maximum cross-sectional diameter is 16 mm. For this system, spectral distortion will result in the aliasing of spectral data from various bands and spaces, which will negatively impact the accuracy of the spectral reconstruction. Thus, the spectral distortion should be less than one pixel.

$$z = \frac{cy^2}{1 + \sqrt{1 - (1+k)c^2y^2}} + \alpha_1 y^2 + \alpha_2 y^4 + \alpha_3 y^6 + \alpha_4 y^8 + \dots \quad (5)$$

In order to correct the spectral distortion, a pair of orthogonal toroid lenses is placed in front of the image. As shown in equation (5), toroidal surfaces are formed by defining a curve in the y - z plane and then rotating this curve about an axis parallel to the y axis and intersecting the z axis. Because of the surface profile of toroidal surface, the nonrotationally symmetric spectral distortion can be corrected effectively. The smile distortion and keystone distortion of the system are 0.0096 mm and 0.01 mm, respectively. The parameters of the two orthogonal toroid surfaces are shown in Table 2.

Figure 4 shows the modulation transfer function (MTF) at three wavelengths: 450 nm, 575 nm, and 700 nm. When the spatial frequency is 52 cycles/mm, the MTF of each field of view (FOV) is above 0.2, which indicates good imaging quality. Through ray tracing, with a spatial interval of $9.6 \mu\text{m}$, Figure 5 depicts the spectrum sampling of various dispersion positions in the central field of view. According to ray tracing data, within the band range of 450~700 nm, the majority of FOVs' spot radius RMS (root

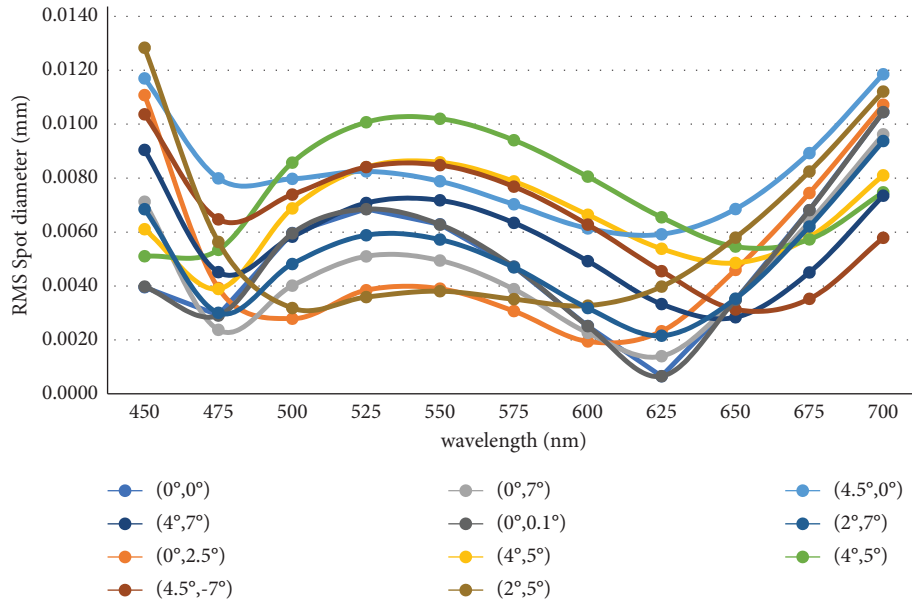


FIGURE 6: Spectral distribution curve of spot radius RMS value under different sampling FOV.

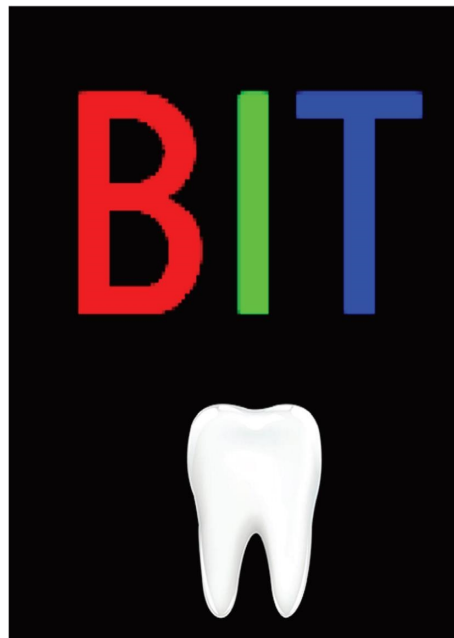


FIGURE 7: Two-dimensional spatial characteristics of target.

mean square) values fall below $9.6 \mu\text{m}$, as shown in Figure 6. Thus, the spectral signals at the focal plane of the detector do not overlap. Based on the above data, if the coding unit size is $9.6 \mu\text{m}$, there are 55 spectral channels. The spectral resolution can be up to 2.2 nm , and as the wavelength increases, the spectral resolution decreases to 10 nm .

4. Simulation of the Snapshot Hyperspectral Dental Imaging Spectrometer

In this section, to verify the feasibility for whiteness measurement by one-dimensional coded snapshot spectral imaging, we conducted simulations of the imaging process and reconstruction process of the system.

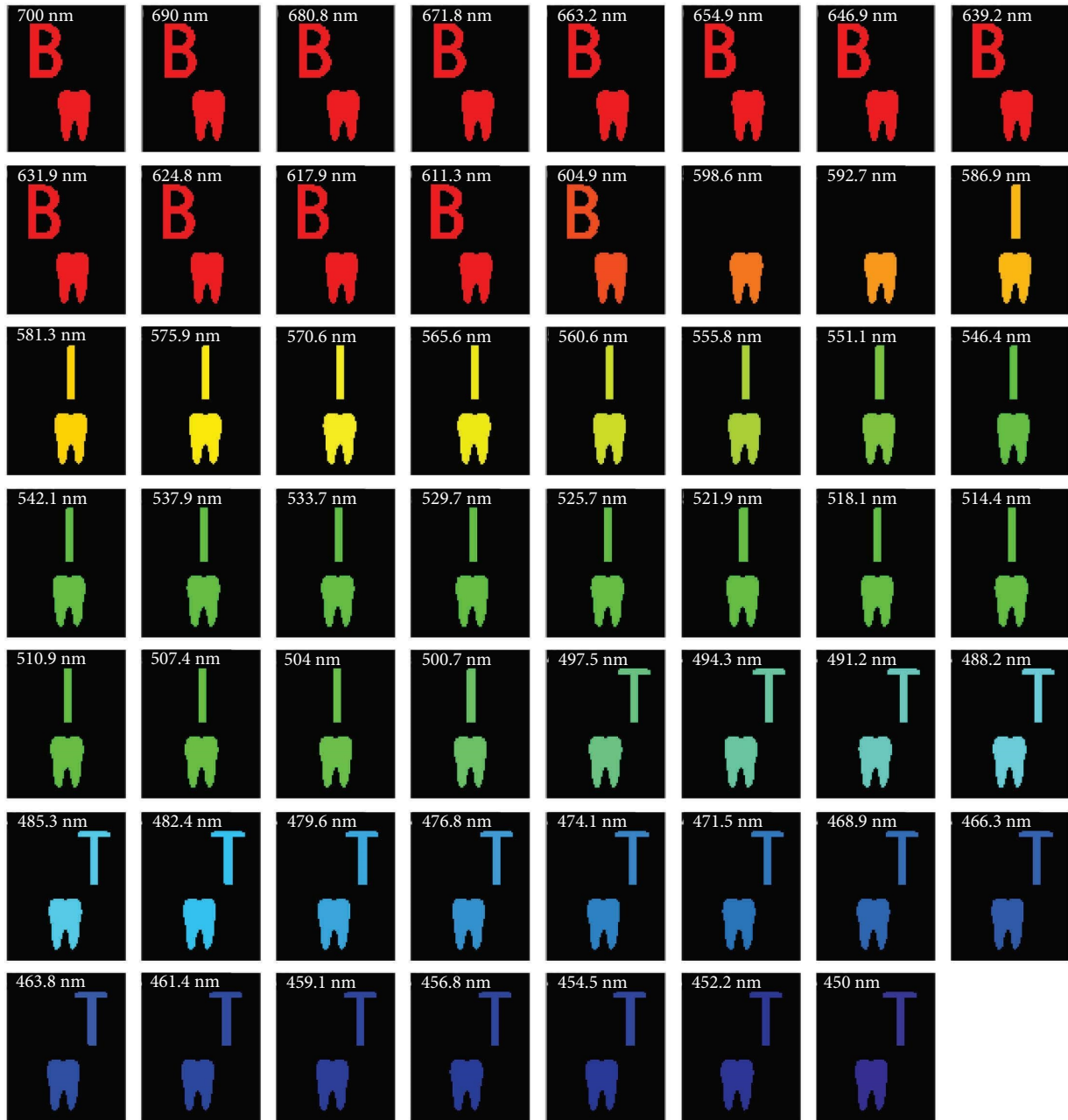


FIGURE 8: Spectral image of target.

A simple model of target with certain spectral characteristics was built as shown in Figures 7 and 8. The target model has the two-dimensional spatial characteristics as shown in Figure 7. In this model, we set up four color regions with different spectral distributions as shown in Figure 8.

In the simulation, a one-dimensional random coding mask with a size of 640×512 pixels was established. Based on ray tracing, the position of the coding mask on the image plane was determined, and a three-dimensional

calibration cube was established. Figure 9 shows the position of the coding mask for six channels (700 nm, 639.2 nm, 604.9 nm, 551.1 nm, 500.7 nm, and 450 nm).

The spectral reconstruction algorithm is another important step. In this paper, we simply used the TwIST (two-step iterative shrinkage/thresholding) algorithm [23] to reconstruct the target spectral data cube. Through the reconstruction algorithm to solve the spectral modulated image shown in Figure 10, the spectral image of target in each channel is shown in Figure 11. The spectral features of

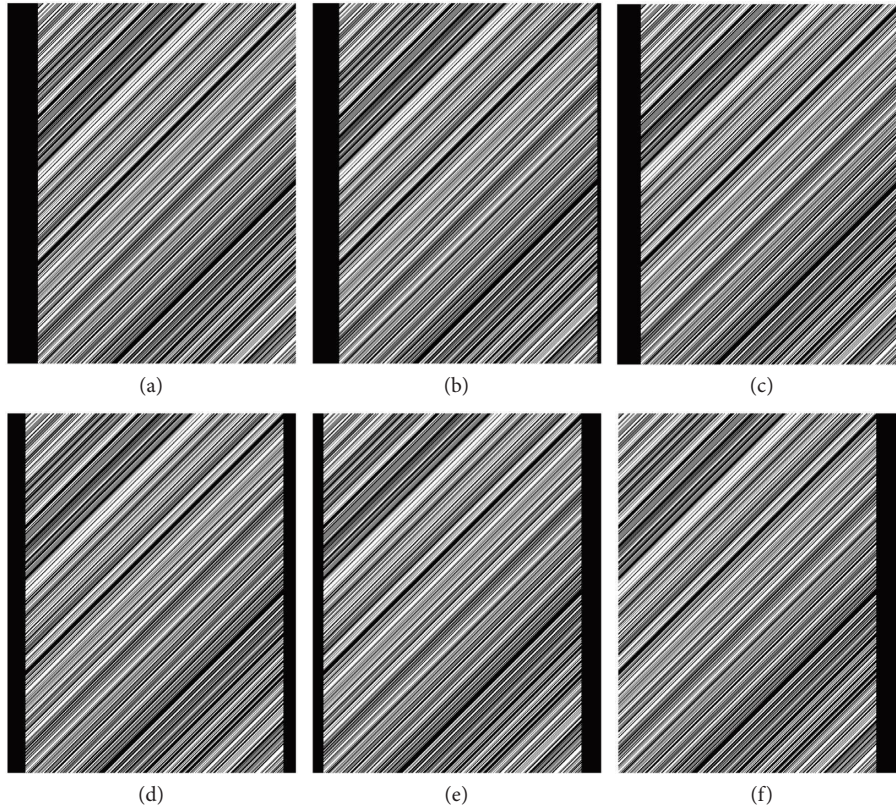


FIGURE 9: Coding mask at six channels: (a) 700 nm, (b) 639.2 nm, (c) 604.9 nm, (d) 551.1 nm, (e) 500.7 nm, and (f) 450 nm.

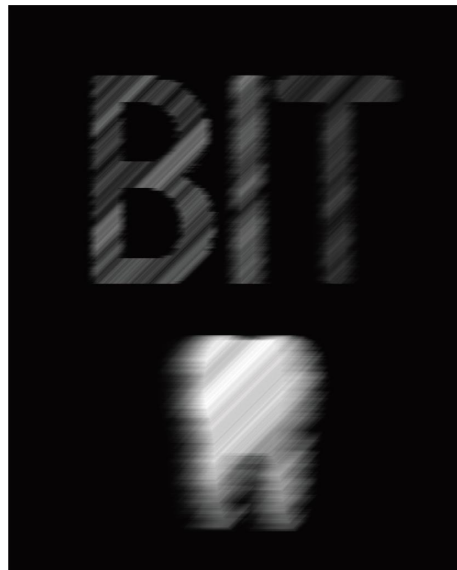


FIGURE 10: Spectral modulated image of the target.

the four regions are distinct, illustrating the feasibility of the proposed snapshot hyperspectral dental imaging spectrometer. The high frequency spatial information in target

reconstruction results is lost, but if the algorithm or coding method is improved, the reconstruction accuracy will be greatly improved.

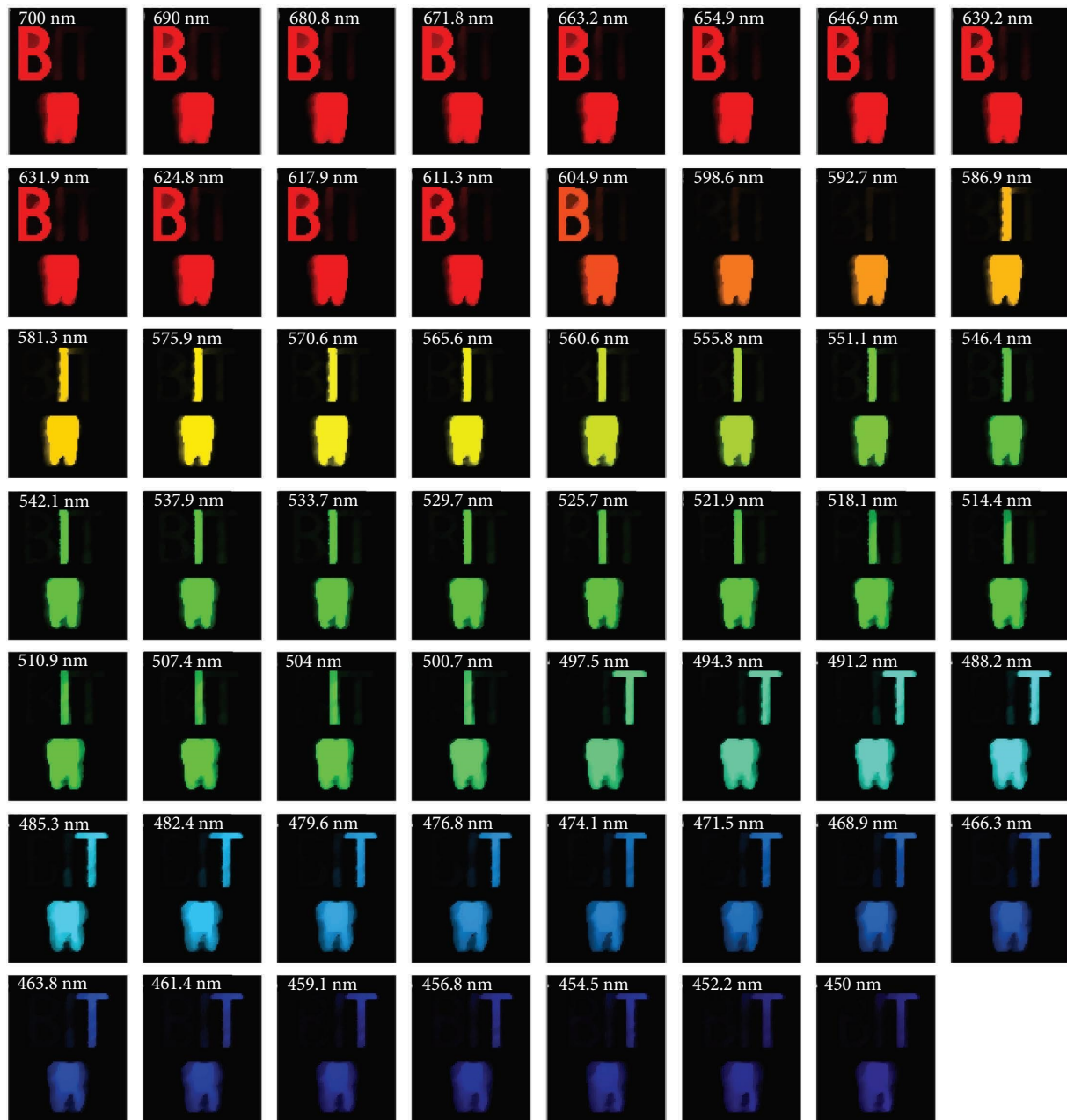


FIGURE 11: Spectral image reconstruction result of target in 55 channels.

5. Conclusion

This article presents the design outline of one-dimensional random coding snapshot hyperspectral dental imaging spectrometer. For the proposed system, we created a transportable optical design. By capturing a picture to reconstruct the target spectrum, the color information of each region may be acquired. With a spectral resolution of 2.2–10 nm, the simulated system successfully yields 55-channel spectral sampling of a 250 nm spectrum within the 450–700 nm spectral region. We have presented the design results and analyzed the imaging performance. A pertinent simulation is run to confirm the viability of one-dimensional coded spectral imaging for measuring whiteness. The simulation

results demonstrated that the snapshot hyperspectral dental imaging spectrometer may solve the problem of teeth and dentures showing the same color under a certain light but with different spectral characteristics.

The proposed system has the potential to improve the accuracy of tooth whiteness measurement. However, there are still some deficiencies in this system at present. No whiteness measurement for real human teeth and verification test has been performed, and no prototype has been successfully produced. Thus, there is still a lot of work to be done in the future. From the results of the current simulations, we believe that if the spectral calibration work is done well and the spectral reconstruction algorithm is strengthened, the precision and accuracy of teeth brightness measurement will be improved.

Data Availability

The data supporting the findings of the study are available upon reasonable request.

Conflicts of Interest

The authors declare that they have no conflicts of interest.

Acknowledgments

This work was supported by the Key Laboratory of Optical System Advanced Manufacturing Technology, Chinese Academy of Sciences (2022KLOMT02-01).

References

- [1] R. D. Paravina, "New shade guide for tooth whitening monitoring: visual assessment," *The Journal of Prosthetic Dentistry*, vol. 99, no. 3, pp. 178–184, 2008.
- [2] Q. Pan and S. Westland, "Tooth color and whitening – digital technologies," *Journal of Dentistry*, vol. 74, pp. S42–S46, 2018.
- [3] A. Mehl, G. Bosch, C. Fischer, and A. Ender, "In vivo tooth-color measurement with a new 3D intraoral scanning system in comparison to conventional digital and visual color determination methods," *International Journal of Computerized Dentistry*, vol. 20, no. 4, pp. 343–361, 2017.
- [4] W. Y. H. Lam, R. T. C. Hsung, L. Y. Y. Cheng, and E. H. N. Pow, "Mapping intraoral photographs on virtual teeth model," *Journal of Dentistry*, vol. 79, pp. 107–110, 2018.
- [5] C. A. Villavicencio-Espinoza, M. H. Narimatsu, and A. Y. Furuse, "Using cross-polarized photography as a guide for selecting resin composite shade," *Operative Dentistry*, vol. 43, no. 2, pp. 113–120, 2018.
- [6] M. Revilla-Leon, M. M. Methani, and M. Özcan, "Impact of the ambient light illuminance conditions on the shade matching capabilities of an intraoral scanner," *Journal of Esthetic and Restorative Dentistry*, vol. 33, no. 6, pp. 906–912, 2020.
- [7] V. Hampé-Kautz, A. Salehi, B. Senger, and O. Etienne, "A comparative in vivo study of new shade matching procedures," *International Journal of Computerized Dentistry*, vol. 23, no. 4, pp. 317–323, 2020.
- [8] J. Ragain, "A review of color science in dentistry: shade matching in the contemporary dental practice," *Journal of Dentistry, Oral Disorders and Therapy*, vol. 4, no. 2, pp. 01–05, 2016.
- [9] F. Tabatabaian, E. Beyabanaki, P. Alirezaei, and S. Epakchi, "Visual and digital tooth shade selection methods, related effective factors and conditions, and their accuracy and precision: a literature review," *Journal of Esthetic and Restorative Dentistry*, vol. 33, no. 8, pp. 1084–1104, 2021.
- [10] R. Ivan and P. Rade, "Color measuring instruments," *Acta Stomatologica Naissi*, vol. 25, no. 60, pp. 925–932, 2009.
- [11] G. Khashayar, A. Dozic, C. J. Kleverlaan, and A. J. Feilzer, "Data comparison between two dental spectrophotometers," *Operative Dentistry*, vol. 37, no. 1, pp. 12–20, 2012.
- [12] S. J. Chu, R. D. Trushkowsky, and R. D. Paravina, "Dental color matching instruments and systems. Review of clinical and research aspects," *Journal of Dentistry*, vol. 38, pp. e2–e16, 2010.
- [13] C. Igiel, K. M. Lehmann, R. Ghinea et al., "Reliability of visual and instrumental color matching," *Journal of Esthetic and Restorative Dentistry*, vol. 29, no. 5, pp. 303–308, 2017.
- [14] S. W. Rais and D. Anastasia, "Shade determination in anterior teeth with spectrophotometer and digital camera in the making of fixed partial dentures:(systematic literature review)," *Sriwijaya Journal of Dentistry*, vol. 3, no. 1, pp. 15–22, 2022.
- [15] P. C. Crespo, A. K. Córdova, A. Palacios, D. Astudillo, and B. Delgado, "Variability in tooth color selection by different spectrophotometers: a systematic review," *The Open Dentistry Journal*, vol. 16, pp. 1–9, 2022.
- [16] Z. Z. Zexia Zhang, J. C. Jun Chang, H. R. Hongxi Ren, K. F. Kaiyuan Fan, and D. L. Dongmei Li, "Snapshot imaging spectrometer based on a microlens array," *Chinese Optics Letters*, vol. 17, no. 1, Article ID 011101, 2019.
- [17] Y. Wang, M. J. Escuti, and M. W. Kudenov, "Snapshot channeled imaging spectrometer using geometric phase holograms," *Optics Express*, vol. 27, no. 11, pp. 15444–15455, 2019.
- [18] J. G. Dwight and T. S. Tkaczyk, "Lenslet array tunable snapshot imaging spectrometer (LATIS) for hyperspectral fluorescence microscopy," *Biomedical Optics Express*, vol. 8, no. 3, pp. 1950–1964, 2017.
- [19] Y. Zhang, S. Zhu, J. Lin, and P. Jin, "High-quality panchromatic image acquisition method for snapshot hyperspectral imaging Fourier transform spectrometer," *Optics Express*, vol. 27, no. 20, pp. 28915–28928, 2019.
- [20] S. Lim, C. Cho, A. Das, and S. Chai, "Coded aperture snapshot imaging based spectral classification," in *Classical Optics*, Optical Society of America Washington, WA, USA, 2014.
- [21] L. Wang, Z. Xiong, D. Gao, G. Shi, and F. Wu, "Dual-camera design for coded aperture snapshot spectral imaging," *Applied Optics*, vol. 54, no. 4, pp. 848–858, 2015.
- [22] H. Zhang, X. Ma, and G. R. Arce, "Compressive spectral imaging approach using adaptive coded apertures," *Applied Optics*, vol. 59, no. 7, pp. 1924–1938, 2020.
- [23] J. Bioucas-Dias, M. Figueiredo, and M. A. T. Figueiredo, "A new TwIST: two-step iterative shrinkage/thresholding algorithms for image restoration," *IEEE Transactions on Image Processing*, vol. 16, no. 12, pp. 2992–3004, 2007.